Proceedings of the ASME 2016 Dynamic Systems and Control Conference
DSCC 2016
October 12 –14, 2016, Minneapolis, Minnesota, USA

DSCC2016-9733

OUTPUT FEEDBACK STABILIZATION OF THE LINEARIZED BILAYER *SAINT-VENANT* MODEL

Ababacar Diagne
Division of Scientific Computing,
Department of Information Technology, Uppsala University,
Box 337, 75105 Uppsala, Sweden
Email: ababacar.diagne@it.uu.se

Shuxia Tang*
Department of Mechanical & Aerospace Engineering,
University of California, San Diego,
La Jolla, CA 92093-0411, USA
Email address: sht015@ucsd.edu

Mamadou Diagne
Department of Mechanical Engineering,
University of Michigan G.G. Brown Laboratory
2350 Hayward Ann Arbor MI 48109, USA
Email address: mdiagne@umich.edu

Miroslav Krstic
Department of Mechanical & Aerospace Engineering,
University of California, San Diego,
La Jolla, CA 92093-0411, USA
Email address: krstic@ucsd.edu

ABSTRACT

We consider the problem of output feedback (exponentially) stabilizing the 1-D bilayer Saint-Venant model, which is a coupled system of two rightward and two leftward convecting transport partial differential equations (PDEs). The PDE backstepping control method is employed. Our designed output feedback controller is based on the observer built in this paper and the state feedback controller designed in [1], where the backstepping control design idea can also be referred to [2] and can be treated as a generalization of the result for the system with constant system coefficients [2] to the one with time-varying coefficients. Numerical simulations of the bilayer Saint-Venant problem are also provided to verify the result.

INTRODUCTION

The dynamics of open-channel hydraulic systems, e.g., estuaries, rivers and irrigation canals, can be modeled by *Saint-Venant* equations. During the past decades, several efforts have been made by engineers and researchers towards the design of control methodologies for the real-time monitoring of open-channel hydraulic systems. In the mean time, many researchers have contributed on the control problem of the *Saint-Venant* equations, e.g., [3].

We consider a 1D bilayer *Saint-Venant* model in this paper, which consists of the superposition of two immiscible fluids with different constant densities. This numerical bilayer model can be derived from the depth-averaged incompressible Navier-Stokes or Euler equations. More details on the derivation of the model could be referred to [4], [5] and [6]. In particular, [6] develops a stable well-balanced time-splitting scheme for a type of bilayer *Saint-Venant* model which satisfies a fully discrete entropy inequality. One can also find some results on mathematical analysis of the related problem in [7] and [8]. Indeed, a numerical solution of the bilayer shallow water equations in two space dimensions is recently presented in [9], based on the Galerkin finite element method. Moreover, Castro, etc. make use of the hydrodynamical flow system in [10] for the computation of maximal and tidally induced bilayer exchange flows through the Strait of Gibraltar which connects the Atlantic Ocean and the Mediterranean Sea. Nevertheless, to the best of the authors' knowledge, there are yet no existing literatures dealing with the relevant output feedback control related problem for this application.

*Corresponding author.

This paper is a continuation of the work [1], in which the full state feedback (exponential) stabilization of a linear version of the 1D bilayer *Saint-Venant* model is achieved by the PDE backstepping control method. PDE backstepping control approach has been successfully employed for the feedback stabilization of various classes of PDEs, e.g., [11, 12], and the objective of this paper is to study the output feedback (exponential) stabilization problem of this model, also by employing the PDE backstepping method. The resulting output feedback controller can unlock the limitation of requiring a full state estimation in [1]. More precisely, we build an exponentially convergent Luenberger observer, which reconstructs the full system state over the domain by employing sensors located only at the upstream. Based on this observer and the full state feedback controller designed in [1], a backstepping output feedback controller is constructed, with which (exponential) stabilization of this system is achieved. Similarly as [1], our backstepping control design idea can also be referred to [2], in which the stabilization problem for a general coupled heterodirectional system of hyperbolic PDEs is solved. This work can be treated as a generalization of the result obtained in [2], from the system with constant system coefficients to the one with time-varying coefficients.

The outline of this paper is as follows. In Section 1, the output feedback control problem is stated. The 1D bilayer *Saint-Venant* model, which consists of two rightward and two leftward convecting transport PDEs, is first formulated based on its physical description, and then a linearized version around a steady state is presented. Section 2 considers a more general system, which consists of m rightward and n leftward transport PDEs with spatially varying coefficients. Subsection 2.1 recalls the state feedback backstepping controller design result in [1], in which the system of the $n+m$ PDEs is exponentially stabilized by m boundary input backstepping controllers. Subection 2.2 designs an observer for this system with only m boundary estimates. Based on the results from these two subsections, Subsection 2.3 constructs a output feedback controller, with which exponential stability is achieved for the closed-loop control system. This general result could serve as a theoretical result by itself, and it can be immediately utilized for the linearized bilayer *Saint-Venant* model, where we achieve (output) feedback exponential stabilization with two boundary input controllers. Numerical simulations are provided in Section 3. Finally in Section 4, a conclusion is presented and some possible future work directions are discussed.

1 Problem Statement

1.1 The 1D nonlinear bilayer *Saint-Venant* model

We consider the (output) feedback stabilization problem of the following 1D bilayer *Saint-Venant* model, which governs the dynamic of two superposed immiscible layers of shallow water fluids:

$$\begin{cases} \dfrac{\partial H_1}{\partial t}+\dfrac{\partial (H_1U_1)}{\partial x}=0, \\ \dfrac{\partial U_1}{\partial t}+U_1\dfrac{\partial U_1}{\partial x}+g\dfrac{\partial H_1}{\partial x}+g\dfrac{\partial H_2}{\partial x}+g\dfrac{\partial B}{\partial x}=S_1^f, \\ \dfrac{\partial H_2}{\partial t}+\dfrac{\partial (H_2U_2)}{\partial x}=0, \\ \dfrac{\partial U_2}{\partial t}+U_2\dfrac{\partial U_2}{\partial x}+g\dfrac{\partial H_2}{\partial x}+g\dfrac{\rho_1}{\rho_2}\dfrac{\partial H_1}{\partial x}+g\dfrac{\partial B}{\partial x}=S_2^f. \end{cases} \tag{1}$$

The index 1 refers to the upper layer and the index 2 to the lower one, as depicted in Figure 1. The unknown state variables H_i, U_i and B represent respectively the thickness of the i-th layer, the velocity and the height of the sediment layer. Each layer is assumed to have a constant density ρ_i, $i=1,2$ ($\rho_1<\rho_2$). The system contains the source terms due to the bottom topography and the friction term. The quantities S_1^f and S_2^f stand as the friction between the two layers, and they are given by

$$S_1^f=-C_f|U_1-U_2|(U_1-U_2) \tag{2}$$

and

$$S_2^f=rC_f|U_1-U_2|(U_1-U_2). \tag{3}$$

Define a vector $W=\left[H_1,\,U_1,\,H_2,\,U_2\right]^T$, a ratio $r=\dfrac{\rho_1}{\rho_2}$ and a map

$$F(W)=\begin{bmatrix} H_1U_1 \\ \dfrac{U_1^2}{2}+g(H_1+H_2) \\ H_2U_2 \\ \dfrac{U_2^2}{2}+g(H_2+rH_1) \end{bmatrix}, \tag{4}$$

then we could recast equation (1) under the form of

$$\frac{\partial W}{\partial t}+\frac{\partial F(W)}{\partial x}=S(x,W), \tag{5}$$

where

$$S(x,W)=\left(0\;\; S_1^f-g\frac{\partial B}{\partial x}\;\; 0\;\; S_2^f-g\frac{\partial B}{\partial x}\right)^T. \tag{6}$$

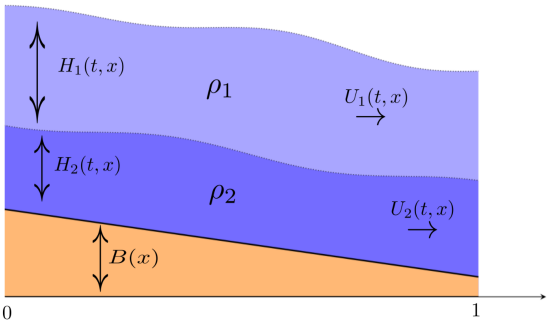

FIGURE 1. Bilayer shallow water flows with variable topography.

By considering the following Jacobian matrix associated with (5):

$$A(W) = \begin{bmatrix} U_1 & H_1 & 0 & 0 \\ g & U_1 & g & 0 \\ 0 & 0 & U_2 & H_2 \\ rg & 0 & g & U_2 \end{bmatrix}, \tag{7}$$

we could rewrite the equation (5) into a quasilinear form as

$$\frac{\partial W}{\partial t} + \boldsymbol{A(W)}\frac{\partial W}{\partial x} = \boldsymbol{S(x,W)}. \tag{8}$$

For the case of $r \approx 1$ and $U_1 \approx U_2$, a first order approximation of the eigenvalues is given in [13, 14]. In this work, we consider the case where $r \ll 1$, namely, when the bottom fluid is much thicker than the upper fluid.

1.2 Linearization of the 1D bilayer *Saint-Venant* model

We denote the steady-state associated to the system (8) by $W^* = (H_1^*, U_1^*, H_2^*, U_2^*)$, which satisfies the following equation of a compact form:

$$\boldsymbol{A(W^*)\partial_x W^* = S(x,W^*)}. \tag{9}$$

In order to obtain a constant steady-state, we work in the sequel with a flat bathymetry ($\partial_x B = 0$). A constant steady-state of the bilayer *Saint-Venant* equations can be then characterized by:

$$\begin{cases} H_1^* U_1^* = \text{constant}, \\ H_2^* U_2^* = \text{constant}, \\ \dfrac{U_1^{*2}}{2} + g(H_1^* + H_2^*) = -C_f |U_1^* - U_2^*|(U_1^* - U_2^*), \\ \dfrac{U_2^{*2}}{2} + g(H_2^* + rH_1^*) = rC_f |U_1^* - U_2^*|(U_1^* - U_2^*). \end{cases} \tag{10}$$

In order to linearize the governing equations, we define the deviation (h_1, u_1, h_2, u_2) of the state (H_1, U_1, H_2, U_2) with respect to the steady-state $(H_1^*, U_1^*, H_2^*, U_2^*)$ by:

$$\begin{cases} h_1 = H_1 - H_1^*, & u_1 = U_1 - U_1^*, \\ h_2 = H_2 - H_2^*, & u_2 = U_2 - U_2^*. \end{cases} \tag{11}$$

Then, the linearized version of (8) can be written in a matrix form as

$$\partial_{\mathbf{t}}\mathbf{U} + \mathbf{A}^*\partial_{\mathbf{x}}\mathbf{U} = \mathbf{S_l}(\mathbf{U}), \tag{12}$$

where

$$U = (h_1, u_1, h_2, u_2)^T, \tag{13}$$
$$A^* = A(W^*), \tag{14}$$

and

$$S_l(U) = [0 \; -\alpha_s^f(u_1 - u_2) \; 0 \; r\alpha_s^f(u_1 - u_2)]^T$$

with

$$\alpha_s^f = 2C_f |U_1^* - U_2^*|.$$

Remark 1. We consider a constant steady state here for the sake of readability and simplicity in the presentation of the linear model. ◦

1.3 Linearized 1D bilayer *Saint-Venant* model in Riemann coordinates

We are to explore the system eigenstructure of the linear form (12) in this subsection. The characteristic equation derived from the matrix A^* is

$$\left((\lambda - U_1^*)^2 - gH_1^*\right)\left((\lambda - U_2^*)^2 - gH_2^*\right) = rg^2 H_1^* H_2^*. \tag{15}$$

For the case of $r = 0$, straightforward calculations lead to the following real eigenvalues for A^*:

$$\begin{aligned} \lambda_1 &= U_1^* - \sqrt{gH_1^*}, & \lambda_2 &= U_1^* + \sqrt{gH_1^*}, \\ \lambda_3 &= U_2^* - \sqrt{gH_2^*}, & \lambda_4 &= U_2^* + \sqrt{gH_2^*}. \end{aligned} \tag{16}$$

We notice that in this case, each eigenvalue corresponds to one specific layer respectively. Following the results in [15], the

eigenvalues for the system (8) in the case of $r \ll 1$ i.e., $\rho_1 \ll \rho_2$ approach to those given in (16). From (16), the internal and external characteristics travel at different speeds, and indeed, the lower layer characteristics moves much slower than the upper ones in the case of $r \ll 1$.

Let us now recast the equation (12) into a diagonal form. For a given eigenvalue λ_k $(k = 1,2,3,4)$ of the matrix A^*, the associated right eigenvector is expressed by

$$V_k = \begin{bmatrix} 1 \\ \dfrac{\lambda_k - U_1^*}{H_1^*} \\ \dfrac{(\lambda_k - U_1^*)^2 - gH_1^*}{gH_1^*} \\ \dfrac{(\lambda_k - U_2^*)((\lambda_k - U_1^*)^2 - gH_1^*)}{gH_1^* H_2^*} \end{bmatrix}. \tag{17}$$

Some computations lead to the associated left eigenvector L_k, which is given by:

$$L_k = -\frac{1}{(\lambda_i - \lambda_k)(\lambda_j - \lambda_k)(\lambda_l - \lambda_k)} \begin{bmatrix} l_{k,1} & l_{k,2} & l_{k,3} & l_{k,4} \end{bmatrix}^T \tag{18}$$

for $i \neq j \neq l \neq k \in \{1,2,3,4\}$, where

$$l_{k,1} = U_1^{*3} - (trA^* - \lambda_k)(U_1^{*2} + gH_1^*) + f_k + 3gH_1^* - \frac{detA^*}{\lambda_k}, \tag{19}$$

$$l_{k,2} = 3H_1^* U_1^{*2} - 2H_1^* U_1^* (trA^* - \lambda_k) + H_1^*(f_k + gH_1^*), \tag{20}$$

$$l_{k,3} = gH_1^*(7U_1^* - \lambda_k), \quad l_{k,4} = gH_1^* H_2^*. \tag{21}$$

The quantities f_k are defined by:

$$f_1 = (\lambda_3 + \lambda_2)\lambda_4 + \lambda_2\lambda_3,\ f_2 = (\lambda_3 + \lambda_1)\lambda_4 + \lambda_1\lambda_3, \tag{22}$$

$$f_3 = (\lambda_2 + \lambda_1)\lambda_4 + \lambda_1\lambda_2,\ f_4 = (\lambda_1 + \lambda_2)\lambda_3 + \lambda_1\lambda_2. \tag{23}$$

We are to express the linear version (12) of the governing equations in term of the characteristic coordinates or Riemann Invariants. Multiplying the equation (12) by the left eigenvectors L_k (each for a given eigenvalue λ_k) of the matrix A^*, we get that the characteristic coordinates (Riemann Invariants) ξ_k are:

$$\xi_k = L_k^{tr} U = -\frac{1}{(\lambda_i - \lambda_k)(\lambda_j - \lambda_k)(\lambda_l - \lambda_k)} \times \Big[l_{k,1} h_1 + l_{k,2} u_1 + l_{k,3} h_2 + l_{k,4} u_2 \Big], \tag{24}$$

for $i \neq j \neq l \neq k \in \{1,2,3,4\}$. Therefore, we can express the variables h_1, u_1, h_2 and u_2 in term of the Riemann coordinates:

$$\begin{cases} h_1 = \xi_1 + \xi_2 + \xi_3 + \xi_4, \\ u_1 = \gamma_1\xi_1 + \gamma_2\xi_2 + \gamma_3\xi_3 + \gamma_4\xi_4, \\ h_2 = \beta_1\xi_1 + \beta_2\xi_2 + \beta_3\xi_3 + \beta_4\xi_4, \\ u_2 = \alpha_1\xi_1 + \alpha_2\xi_2 + \alpha_3\xi_3 + \alpha_4\xi_4, \end{cases} \tag{25}$$

where

$$\gamma_k = \frac{\lambda_k - 1}{H_1^*}, \tag{26}$$

$$\beta_k = \frac{1}{gH_1^*}\Big(U_1^{*2} + 2(\lambda_k - 1)U_1^* - \lambda_k^2 + gH_1^* \Big), \tag{27}$$

and

$$\begin{aligned} \alpha_k = & \frac{1}{gH_1^* H_2^*}\big((gH_1^*\beta_k - 2\lambda_k^2)U_2^* + 3U_1^{*3} \\ & + 7(\lambda_k - 1)U_1^{*2} + 2(gH_1^* - 2\lambda_k^2)U_1^* \\ & + \lambda_k^2(trA^* - \lambda_k) + gH_1^*(\lambda_k + 2) \big). \end{aligned} \tag{28}$$

Introduce the following more compact notations:

$$\boldsymbol{\xi} = \begin{pmatrix} \xi_1 & \xi_2 & \xi_3 & \xi_4 \end{pmatrix}^{tr},\ \boldsymbol{\Lambda} = \mathrm{diag}\{\lambda_1, \lambda_2, \lambda_3, \lambda_4\}, \tag{29}$$

then, by using the characteristic coordinates, we recast the equation (12) into the following form:

$$\boldsymbol{\partial_t \xi + \Lambda \partial_x \xi = M \xi}, \tag{30}$$

where

$$\begin{aligned} M(W^*) = & \begin{pmatrix} 0 & \alpha_s^f & 0 & -r\alpha_s^f \end{pmatrix}^{tr} \\ & \times \begin{pmatrix} \alpha_1 - \gamma_1 & \alpha_2 - \gamma_2 & \alpha_3 - \gamma_3 & \alpha_4 - \gamma_4 \end{pmatrix}. \end{aligned} \tag{31}$$

We consider the case where both layers have a subcritical flow regime. Define the state vectors

$$u(t,x) = (\xi_2, \xi_4),\ v(t,x) = (\xi_1, \xi_3),$$

and introduce the transport speed matrices

$$\boldsymbol{\Lambda}^{\mathrm{r}} = \mathrm{diag}\{\lambda_2, \lambda_4\},\ -\boldsymbol{\Lambda}^{\mathrm{l}} = \mathrm{diag}\{\lambda_1, \lambda_3\}.$$

Then, the system (30) can be rewritten as

$$\partial_t u(t,x) + \Lambda^{\mathrm{r}} \partial_x u(t,x) = S^{\mathrm{r}} u(t,x) + S^{\mathrm{l}} v(t,x), \tag{32}$$
$$\partial_t v(t,x) - \Lambda^{\mathrm{l}} \partial_x v(t,x) = 0, \tag{33}$$

where

$$S^{\mathrm{r}} = \begin{bmatrix} \alpha_s^f(\alpha_1 - \gamma_1) & \alpha_s^f(\alpha_2 - \gamma_2) \\ r\alpha_s^f(\gamma_1 - \alpha_1) & r\alpha_s^f(\gamma_2 - \alpha_2) \end{bmatrix}, \tag{34}$$
$$S^{\mathrm{l}} = \begin{bmatrix} \alpha_s^f(\alpha_3 - \gamma_3) & \alpha_s^f(\alpha_4 - \gamma_4) \\ r\alpha_s^f(\gamma_3 - \alpha_3) & r\alpha_s^f(\gamma_4 - \alpha_4) \end{bmatrix}. \tag{35}$$

To close the writing of the system (32)-(33), we enclose to it the following boundary and initial conditions:

$$u(t,0) = Q_0 v(t,0) \tag{36}$$
$$v(t,1) = R_1 u(t,1) + \mathfrak{U}(t) \tag{37}$$
$$u(0,x) = u_0(x) \tag{38}$$
$$v(0,x) = v_0(x), \tag{39}$$

where Q_0, $R_1 \in \mathscr{M}_{2,2}(\mathbb{R})$, and $\mathfrak{U}(t) = (\mathfrak{u}_1(t), \mathfrak{u}_2(t))$ consists of the boundary controllers we need to design.

2 Controller design of a general system

In this section, we consider the output feedback controller design of the following more general system discussed in [1]:

$$\partial_t u(t,x) + \Lambda^{\mathrm{r}}(x) \partial_x u(t,x) = S^{\mathrm{r}}(x) u(t,x) + S^{\mathrm{l}}(x) v(t,x), \tag{40}$$
$$\partial_t v(t,x) - \Lambda^{\mathrm{l}}(x) \partial_x v(t,x) = S^{\mathrm{o}}(x) u(t,x), \tag{41}$$
$$u(t,0) = Q_0 v(t,0), \tag{42}$$
$$v(t,1) = R_1 u(t,1) + \mathfrak{U}(t), \tag{43}$$
$$u(0,x) = u_0(x), \tag{44}$$
$$v(0,x) = v_0(x), \tag{45}$$

where

$$u(x,t) = \left[u_1(x,t), u_2(x,t), \ldots, u_n(x,t)\right], \tag{46}$$
$$v(x,t) = \left[v_1(x,t), v_2(x,t), \ldots, v_m(x,t)\right] \tag{47}$$

are the system states. The matrices

$$\mathbf{\Lambda}^{\mathrm{r}}(x) = \mathrm{diag}\left[\lambda_1^{\mathrm{r}}(x), \lambda_2^{\mathrm{r}}(x), \cdots, \lambda_n^{\mathrm{r}}(x)\right], \tag{48}$$
$$\mathbf{\Lambda}^{\mathrm{l}}(x) = \mathrm{diag}\left[\lambda_1^{\mathrm{l}}(x), \lambda_2^{\mathrm{l}}(x), \cdots, \lambda_m^{\mathrm{l}}(x)\right], \tag{49}$$

where

$$0 < \lambda_1^{\mathrm{r}}(x) < \lambda_2^{\mathrm{r}}(x) < \cdots < \lambda_n^{\mathrm{r}}(x), \tag{50}$$
$$-\lambda_m^{\mathrm{l}}(x) < -\lambda_2^{\mathrm{l}}(x) \cdots < -\lambda_1^{\mathrm{l}}(x) < 0, \tag{51}$$

and the in-domain parameters are given as

$$S^{\mathrm{r}}(x) = \{S_{ij}^{\mathrm{r}}(x)\}_{1\le i\le n, 1\le j\le n}, \tag{52}$$
$$S^{\mathrm{l}}(x) = \{S_{ij}^{\mathrm{l}}(x)\}_{1\le i\le n, 1\le j\le m}, \tag{53}$$
$$S^{\mathrm{o}}(x) = \{S_{ij}^{\mathrm{o}}(x)\}_{1\le i\le n, 1\le j\le m}. \tag{54}$$

The boundary parameters Q_0, $R_1 \in \mathscr{M}_{m,n}(\mathbb{R})$ are given as

$$R_1 = \{r_{ij}\}_{1\le i\le m, 1\le j\le n}, \quad Q_0 = \{q_{ij}(x)\}_{1\le i\le n, 1\le j\le m}, \tag{55}$$

and the boundary controllers are given as

$$\mathfrak{U}(t) = \left[\mathfrak{u}_1(t)\ \mathfrak{u}_2(t)\ \ldots\ \mathfrak{u}_n(t)\right]^T. \tag{56}$$

The system (40) – (45) could includes the *Saint-Venant* model as a special case. While solving our problem with the *Saint-Venant* model, the result derived in this section could also be treated as a full theoretical result by itself.

2.1 State feedback control design result

The PDE backstepping method is employed. We recall from [1] that a backstepping transformation is constructed:

$$\begin{pmatrix} \varepsilon(t,x) \\ \beta(t,x) \end{pmatrix} = \begin{pmatrix} u(t,x) \\ v(t,x) \end{pmatrix} - \int_0^x \begin{pmatrix} 0 & 0 \\ G_{21}(x,\xi) & G_{22}(x,\xi) \end{pmatrix} \begin{pmatrix} u(t,\xi) \\ v(t,\xi) \end{pmatrix} d\xi, \tag{57}$$

where the kernels G_{21} and G_{22} are defined on the domain $\mathbb{T} = \left\{(x,\xi) \in \mathbb{R}^2 |\ 0 \le \xi \le x \le 1\right\}$ and satisfy the following system of equations:

$$\partial_\xi G_{21}(x,\xi)\mathbf{\Lambda}^{\mathrm{r}}(\xi) - \mathbf{\Lambda}^{\mathrm{l}}(x)\partial_x G_{21}(x,\xi) = -G_{21}(x,\xi)\frac{d\mathbf{\Lambda}^{\mathrm{r}}(\xi)}{d\xi} - G_{21}(x,\xi)S^{\mathrm{r}}(\xi) - G_{22}(x,\xi)S^{\mathrm{o}}(\xi) \tag{58}$$
$$\partial_\xi G_{22}(x,\xi)\mathbf{\Lambda}^{\mathrm{r}}(\xi) + \mathbf{\Lambda}^{\mathrm{l}}(x)\partial_x G_{22}(x,\xi) = -G_{22}(x,\xi)\frac{d\mathbf{\Lambda}^{\mathrm{r}}(\xi)}{d\xi} + G_{21}(x,\xi)S^{\mathrm{l}}(\xi), \tag{59}$$
$$G_{21}(x,x)\mathbf{\Lambda}^{\mathrm{r}}(x) + \mathbf{\Lambda}^{\mathrm{l}}(x)G_{21}(x,x) = -S^{\mathrm{o}}(x), \tag{60}$$
$$G_{22}(x,x)\mathbf{\Lambda}^{\mathrm{l}}(x) - \mathbf{\Lambda}^{\mathrm{l}}(x)G_{22}(x,x) = 0, \tag{61}$$
$$G_{21}(x,0)\mathbf{\Lambda}^{\mathrm{r}}(0)Q_0 - G_{22}(x,0)\mathbf{\Lambda}^{\mathrm{l}}(0) = -\Delta(x). \tag{62}$$

Here,

$$\Delta(x)=\begin{bmatrix} 0 & \cdots & \cdots & 0 \\ \delta_{2,1}(x) & \ddots & \ddots & \vdots \\ \vdots & \ddots & \ddots & \vdots \\ \delta_{m,1}(x) & \cdots & \delta_{m,m-1}(x) & 0 \end{bmatrix}, \tag{63}$$

where $\delta_{i,j}(x), i=\overline{2,\ m},\ j=\overline{1,\ m-1}$ are obtained from the inverse transformation of (57).

The transformation (57) maps the closed-loop control system (40) – (45), with a full state feedback backstepping controller

$$\mathfrak{U}(t)=-R_1u(t,1)+\int_0^1[G_{21}(1,\xi)u(t,\xi)+G_{22}(1,\xi)v(t,\xi)]d\xi, \tag{64}$$

into an exponential stable target system

$$\begin{aligned}&\partial_t\varepsilon(t,x)+\Lambda^{\mathrm{r}}(x)\partial_x\varepsilon(t,x)=S^{\mathrm{r}}(x)\varepsilon(t,x)+S^{\mathrm{l}}(x)\beta(t,x)\\&+\int_0^x C^{\mathrm{r}}(x,\xi)\varepsilon(\xi)d\xi+\int_0^x C^{\mathrm{l}}(x,\xi)\beta(\xi)d\xi \qquad (65)\\&\partial_t\beta(t,x)-\Lambda^{\mathrm{l}}(x)\partial_x\beta(t,x)=\Delta(x)\beta(0,t) \qquad (66)\\&\varepsilon(t,0)=Q_0\beta(t,0) \qquad (67)\\&\beta(t,1)=0. \qquad (68)\end{aligned}$$

With the exponential stability of the target system, and with existence, regularity and invertibility of the backstepping tranformation, the stability of the closed-loop control system is then derived. We also recall the following main theorem in [1].

Theorem 1. *For any given initial data* $(u^0,\ v^0)^T=(u(0,\cdot),\ v(0,\cdot))^T\in\left(\mathscr{L}^2([0,1])\right)^{n+m}$ *and under the assumption that* $C^{\mathrm{r}},\ C^{\mathrm{l}}\in\mathscr{C}(\mathbb{T})$*, the equilibrium* $(u,\ v)^T=(0,\ 0,\ 0,\ 0)^T$ *of the closed-loop system (40) –* (45) *with the designed controller* (64) *is exponentially stable in the sense of* $\mathscr{L}^2$*-norm:*

$$\|(u(t,\cdot),v(t,\cdot))\|^2_{\mathscr{L}^2}:=\int_0^1 u^T(t,x)u(t,x)+v^T(t,x)v(t,x)dx. \tag{69}$$

2.2 Backstepping observer design

The backstepping controller (64) requires a full state measurement across the spatial domain. In this section we design a boundary state observer for estimating the distributed states of the system (40)–(45) over the whole spatial domain using the measured output $y(t)=v(t,0)$, which could help avoid the full state measurement in a to-be-designed output feedback controller.

Consider the following state observer, which consists of a copy of the plant (40)–(45) plus output injection terms:

$$\begin{aligned}&\partial_t\hat{u}+\Lambda^{\mathrm{r}}(x)\partial_x\hat{u}=S^{\mathrm{r}}(x)\hat{u}+S^{\mathrm{l}}(x)\hat{v}-P_1(x)[y(t)-\hat{v}(t,0)], \qquad (70)\\&\partial_t\hat{v}-\Lambda^{\mathrm{l}}(x)\partial_x\hat{v}=S^{\mathrm{o}}(x)\hat{u}-P_2(x)[y(t)-\hat{v}(t,0)], \qquad (71)\\&\hat{u}(t,0)=Q_0y(t), \qquad (72)\\&\hat{v}(t,1)=R_1\hat{u}(t,1)+\mathfrak{U}(t). \qquad (73)\end{aligned}$$

Here, $(\hat{u},\hat{v})^T$ is the estimated state vector, and the output injection coefficients $P_1(x)$ and $P_2(x)$ are to be determined so that the estimated state vector $(\hat{u},\ \hat{v})$ converges to the real state vector (u,v).

Let $\left(\tilde{u}\ \tilde{v}\right)^T=\left(u-\hat{u}\ v-\hat{v}\right)^T$, then we obtain the following observer error system:

$$\begin{aligned}&\partial_t\tilde{u}+\Lambda^{\mathrm{r}}(x)\partial_x\tilde{u}=S^{\mathrm{r}}(x)\tilde{u}+S^{\mathrm{l}}(x)\tilde{v}+P_1(x)\tilde{v}(t,0), \qquad (74)\\&\partial_t\tilde{v}-\Lambda^{\mathrm{l}}(x)\partial_x\tilde{v}=S^{\mathrm{o}}(x)\tilde{u}+P_2(x)\tilde{v}(t,0), \qquad (75)\\&\tilde{u}(t,0)=0, \qquad (76)\\&\tilde{v}(t,1)=R_1\tilde{u}(t,1). \qquad (77)\end{aligned}$$

2.2.1 Backstepping transformation and the target system

We use the following invertible backstepping transformation

$$\begin{aligned}&\tilde{u}(t,x)=\tilde{\varepsilon}(t,x)+\int_0^x M(x,\xi)\tilde{\beta}(t,\xi)\,d\xi, \qquad (78)\\&\tilde{v}(t,x)=\tilde{\beta}(t,x)+\int_0^x N(x,\xi)\tilde{\beta}(t,\xi)\,d\xi, \qquad (79)\end{aligned}$$

where the kernels M and N are defined on the triangular domain $\mathbb{T}$ to map the error system (74)–(77) into the following exponentially stable target system

$$\begin{aligned}&\partial_t\tilde{\varepsilon}+\Lambda^{\mathrm{r}}(x)\partial_x\tilde{\varepsilon}=S^{\mathrm{r}}(x)\tilde{\varepsilon}+\int_0^x D^r(x,\xi)\tilde{\varepsilon}(t,\xi)\,d\xi, \qquad (80)\\&\partial_t\tilde{\beta}-\Lambda^{\mathrm{l}}(x)\partial_x\tilde{\beta}=S^{\mathrm{o}}(x)\tilde{\varepsilon}+\int_0^x D^l(x,\xi)\tilde{\varepsilon}(t,\xi)\,d\xi, \qquad (81)\\&\tilde{\varepsilon}(t,0)=0, \qquad (82)\\&\tilde{\beta}(t,1)=R_1\tilde{\varepsilon}(t,1)-\int_0^1\tilde{\Delta}(\xi)\tilde{\beta}(t,\xi)d\xi. \qquad (83)\end{aligned}$$

Here, the functions $D^r(x,\xi), D^l(x,\xi)$ and $\tilde{\Delta}(\xi)$ are to be determined later.

Through some lengthy calculations and integrations by parts, the following PDEs are derived for the transformation kernels $M(x,\xi)$ and $N(x,\xi)$:

$$-[M_\xi(x,\xi)\Lambda^{\mathrm{l}}(\xi)+M(x,\xi)(\Lambda^{\mathrm{l}})'(\xi)]+\Lambda^{\mathrm{r}}(x)M_x(x,\xi) = S^{\mathrm{r}}(x)M(x,\xi)+S^{\mathrm{l}}(x)N(x,\xi), \quad (84)$$

$$-[N_\xi(x,\xi)\Lambda^{\mathrm{l}}(\xi)+N(x,\xi)(\Lambda^{\mathrm{l}})'(\xi)]-\Lambda^{\mathrm{l}}(x)N_x(x,\xi) = S^{\mathrm{o}}(x)M(x,\xi), \quad (85)$$

$$M(x,x)\Lambda^{\mathrm{l}}(x)+\Lambda^{\mathrm{r}}(x)M(x,x) = S^{\mathrm{l}}(x), \quad (86)$$

$$N(x,x)\Lambda^{\mathrm{l}}(x)-\Lambda^{\mathrm{l}}(x)N(x,x) = 0. \quad (87)$$

In the mean time, we derive that the observer gains can be defined by

$$P_1(x) = -M(x,0)\Lambda^{\mathrm{l}}(0),\ P_2(x) = -N(x,0)\Lambda^{\mathrm{l}}(0), \quad (88)$$

and the functions $D^r(x,\xi), D^l(x,\xi)$ and $\tilde{\Delta}(\xi)$ are defined by the following equations:

$$D^r(x,\xi)+M(x,\xi)S^{\mathrm{o}}(\xi)+\int_\xi^x M(x,\eta)D^l(\eta,\xi)d\eta = 0, \quad (89)$$

$$D^l(x,\xi)+N(x,\xi)S^{\mathrm{o}}(\xi)+\int_\xi^x N(x,\eta)D^l(\eta,\xi)d\eta = 0, \quad (90)$$

$$\tilde{\Delta}(\xi) = N(1,\xi)-R_1M(1,\xi). \quad (91)$$

2.2.2 Inverse Transformation

The regularity of the transformation (78)–(79) can be discussed by following [2], and then the continuity of the kernels guarantees the existence of a unique inverse transformation. We write the inverse transformation as

$$\tilde{\varepsilon}(t,x) = \tilde{u}(t,x)+\int_0^x \mathscr{M}(x,\xi)\tilde{v}(t,\xi)\,d\xi, \quad (92)$$

$$\tilde{\beta}(t,x) = \tilde{v}(t,x)+\int_0^x \mathscr{N}(x,\xi)\tilde{v}(t,\xi)\,d\xi, \quad (93)$$

with which we then immediately have from (78)–(79) that

$$\tilde{\varepsilon}(t,x) = \tilde{\varepsilon}(t,x)+\int_0^x M(x,\xi)\tilde{\beta}(t,\xi)\,d\xi + \int_0^x \mathscr{M}(x,\xi)[\tilde{\beta}(t,\xi)+\int_0^\xi N(\xi,\eta)\tilde{\beta}(t,\eta)\,d\eta]d\xi, \quad (94)$$

$$\tilde{\beta}(t,x) = \tilde{\beta}(t,x)+\int_0^x N(x,\xi)\tilde{\beta}(t,\xi)\,d\xi + \int_0^x \mathscr{N}(x,\xi)[\tilde{\beta}(t,\xi)+\int_0^\xi N(\xi,\eta)\tilde{\beta}(t,\eta)\,d\eta]\,d\xi. \quad (95)$$

Thus, the kernels $\mathscr{M}(x,\xi), \mathscr{N}(x,\xi)$ need to satisfy

$$0 = M(x,\xi)+\mathscr{M}(x,\xi)+\int_\xi^x \mathscr{M}(x,\eta)N(\eta,\xi)d\eta$$

$$0 = N(x,\xi)+\mathscr{N}(x,\xi)+\int_\xi^x \mathscr{N}(x,\eta)N(\eta,\xi)d\eta. \quad (96)$$

For solving the above system of equations, we could use the method of successive approximations [12, Section 4.4].

2.2.3 Stability of the target system and convergence of the designed observer

We could prove exponential stability of the target system (80)–(83), by following the idea in [1] and employing a Lyapunov function in which the parameters need to be successively determined.

Lemma 1. *For any given data* $((\tilde{\varepsilon}^0)^T,(\tilde{\beta}^0)^T)^T \in (\mathscr{L}^2([0,1]))^{n+m}$, *the system* (80) – *(83), with* (84)–(87), (89)–(91)*, is exponentially stable in the* $\mathscr{L}^2$ *sense:*

$$\|(\tilde{\varepsilon}(t,\cdot),\tilde{\beta}(t,\cdot))\|^2_{\mathscr{L}^2} := \int_0^1 \tilde{\varepsilon}^T(t,x)\tilde{\varepsilon}(t,x)+\tilde{\beta}^T(t,x)\tilde{\beta}(t,x)dx. \quad (97)$$

Furthermore, for any given data $((u^0)^T,\ (v^0)^T,\ (\hat{u}^0)^T,\ (\hat{v}^0)^T)^T \in (\mathscr{L}^2([0,1]))^{2(n+m)}$, *the observer* (70)–(73) *exponentially converges to the system* (40)–(45) *in the* $\mathscr{L}^2$ *sense:*

$$\|(u-\hat{u},v-\hat{v})\|^2_{\mathscr{L}^2} := \int_0^1 (u-\hat{u})^T(u-\hat{u})+(v-\hat{v})^T(v-\hat{v})dx. \quad (98)$$

The proof is omitted here.

2.3 Output feedback controller design

Based on the backstepping controller designed in [1], which requires a full state measurement, and the observer (73), which reconstructs the state over the whole spatial domain through the boundary measurement $v(t,0)$, we could design an observer-based output feedback controller.

Theorem 2. *For any given initial data* $((u^0)^T,\ (v^0)^T,\ (\hat{u}^0)^T,\ (\hat{v}^0)^T)^T \in (\mathscr{L}^2([0,1]))^{2(n+m)}$, *the closed-loop* $(u^T,\ v^T,\ \hat{u}^T,\ \hat{v}^T)^T$*-system* (40)–(45), (70)–(73), *where the observer is defined by* (84)–(88) *and the control law shown in* (43)–(73) *is*

$$\mathfrak{U}(t) = -R_1\hat{u}(t,1) + \int_0^1 \Big[G_{21}(1,\xi)\hat{u}(t,\xi)+G_{22}(1,\xi)\hat{v}(t,\xi)\Big]d\xi \quad (99)$$

with the kernels G_{21} and G_{22} defined by (58)–(63)*, is exponentially stable in the sense of the $\mathscr{L}^2$-norm:*

$$\|(u(t,\cdot),v(t,\cdot),\hat{u}(t,\cdot),\hat{v}(t,\cdot))\|^2_{\mathscr{L}^2} := \int_0^1 \Big[u^T(t,x)u(t,x) + v^T(t,x)v(t,x) + \hat{u}^T(t,x)\hat{u}(t,x) + \hat{v}^T(t,x)\hat{v}(t,x)\Big]dx. \tag{100}$$

The proof is omitted here, for which the the Lyapunov function can be constructed in a similar fashion as in [1] .

3 Simulation results

The goal of the following numerical simulations is to illustrate the efficiency of the designed $\mathfrak{U}(t)$, namely (64), to stabilize the linear system (30) around the zero equilibrium. The following data are considered as initial conditions for the layer 1 and 2 through the physical variables:

$$H_2(0,x) = 2 + 0.5\exp\Big(-\frac{(x-0.5)^2}{0.003}\Big), H_1(0,x) = 6 - H_1(x)$$

and

$$U_1(0,x) = \frac{10}{H_1(0,x)} + 3\sin(2\pi x),$$

$$U_2(0,x) = -\frac{10}{H_2(0,x)} - 3\sin(2\pi x).$$

The initial data of the characteristic variables ξ_k, $(k = 1, 2, 3, 4)$ (for system (30)) are computed as function of the physical variables $H_i(0,x)$ and $U_i(0,x)$ for $i = 1, 2$, thanks to the relation (18). For the sake of simplicity, we consider the following uniform steady state:

$$H_1^* = 3,\ U_1^* = 1, H_2^* = 1, U_2^* = 0.95.$$

With this choice of steady state (set point), the characteristic speeds are given by:

$$\lambda_1 = 6.42,\ \lambda_2 = 4.08,\ \lambda_3 = -4.42 \text{ and } \lambda_4 = -2.18.$$

Elsewhere, in the reported numerical experiments, the ratio r between the densities is set to 0.01 and the friction coefficient C_f to 0.05. We compute the solution up to time $T = 10$. Regarding to the boundary conditions (45), the following matrix are considered:

$$Q_0 = \begin{bmatrix} -1.5 & 0.01 \\ 0.01 & 1.5 \end{bmatrix}, \quad R_1 = \begin{bmatrix} 0.5 & 0.1 \\ 0.15 & -0.5 \end{bmatrix} \tag{101}$$

Our implementation is based on an accurate finite volume method for the evolution equation (30). More precisely, we use a modified Roe's scheme (see, [16]). Since the computation of the designed control $\mathfrak{U}(t)$ requires the knowledge of the kernels G_{21} and G_{22}, we solve the kernels numerically according to (58)–(63) using the finite element setup. As an illustration, the numerical solution of the second component of the kernel G_{21} is given in Figure 2.

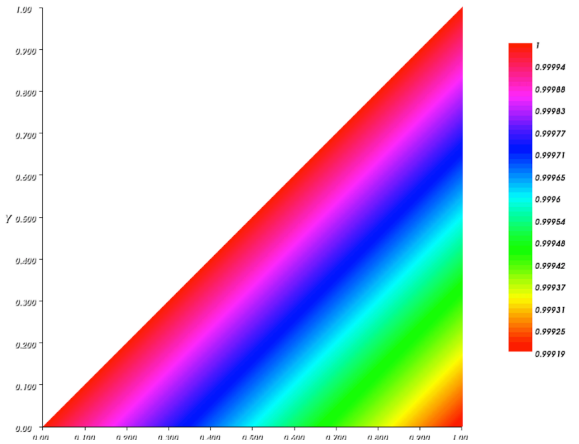

FIGURE 2. The second component of kernel G_{21} ($G_{21}(1,2)$).

In Figure 3, the behavior in time of each component of the input control $\mathfrak{U}(t)$ are depicted. Clearly, despite the initial amplitudes, the second component of the control input $u_2(t)$ decreases in time and vanishes after $t \geq 4s$, and the first component of the control input $u_1(t)$ shows a similar trend, with its amplitude decreasing in time and tending to zero after $t \geq 7s$.

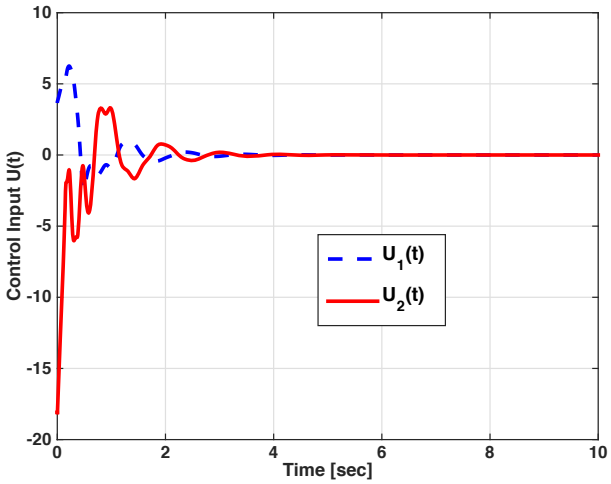

FIGURE 3. Evolution of the component of the control input $U(t)$.

Figure 4 depicts the evolution in time of the $\mathscr{L}^2$-norm of the characteristics. As expected from the theoretical part we observe clearly that the norm of all characteristics decreases in time and converges to zero. As a result, this shows that the system (30) subjected to the feedback control $\mathfrak{U}(t)$ converges to the zero equilibrium. Thereby, the bilayer *Saint-Venant* model (1) is stabilized around the steady state $(H_1^*, U_1^*, H_2^*, U_2^*)$.

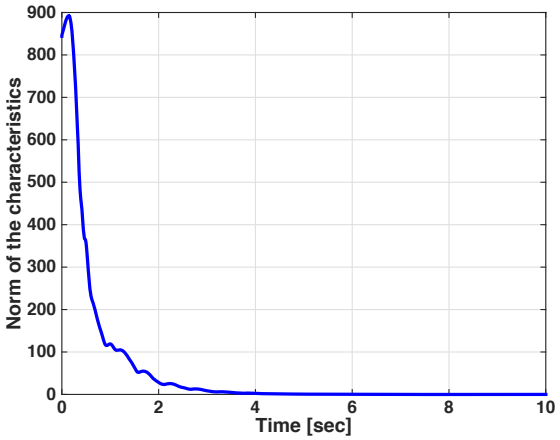

FIGURE 4. Evolution of the norm of the characteristic solutions.

4 Conclusion and Future Works

In this paper, a general system with spatially varying coefficients, consisting of m rightward and n leftward convecting transport PDEs, is exponentially stabilized by m output feedback backstepping boundary controllers, with the help of an observer through m boundary estimates. Our control design idea can be referred to an existing result for a special case (with constant coefficients) [2] of this system, and this result can be considered as a generalization of the one for the special case. Then, it is immediately applied to exponentially stabilize a 1D linearized bilayer *Saint-Venant* model, which is a coupled system of two rightward and two leftward convecting transport PDEs.

It is worth noting that such systems are subjected to several types of perturbations and model uncertainties. Thus, an effective control action must take into account of these factors. One of our next steps is to consider the stabilization problem of the 1D linearized bilayer *Saint-Venant* model with matched disturbance at the boundary input, and the control methods we are going to utilize are the sliding mode control method [17, 18] and the active disturbance rejection control method [19]. Another one of our future works is to consider robustness issues for this application.

REFERENCES

[1] Diagne, A., Tang, S., Diagne, M., and Krstic, M., 2015. "State feedback stabilization of the linearized bilayer *Saint-Venant* model ". *Submitted to the 2nd IFAC Workshop on Control of Systems Modeled by Partial Differential Equations, under review*.

[2] Hu, L., Meglio, F. D., Vazquez, R., and Krstic, M., 2015. "Control of homodirectional and general heterodirectional linear cou- pled hyperbolic pdes". *arXiv preprint arXiv:1504.07491*.

[3] Diagne, A., Diagne, M., Tang, S., and Krstic, M., 2015. "Backstepping stabilization of the linearized *Saint-Venant* model". *Submitted to Automatica, under review*.

[4] Castro, J. M., Garcıa-Rodrıguez, J. A., González-Vida, J. M., Macıas, J., Parés, C., and Vázquez-Cendón, M. E., 2004. "Numerical simulation of two-layer shallow water flows through channels with irregular geometry". *Journal of Computational Physics,* ***195***(1), pp. 202–235.

[5] Audusse, E., Bristeau, M.-O., Perthame, B., and Sainte-Marie, J., 2011. "A multilayer saint-venant system with mass exchanges for shallow water flows. derivation and numerical validation". *ESAIM: Mathematical Modelling and Numerical Analysis,* ***45***(1), 1, pp. 169–200.

[6] Bouchut, F., and Morales, d. L. T., 2008. "An entropy satisfying scheme for two-layer shallow water equations with uncoupled treatment". *ESAIM: Mathematical Modelling and Numerical Analysis,* ***42***, 7, pp. 683–698.

[7] Narbona-Reina, G., and Zabsonre, J. D. D., 2009. "Existence of a global weak solution for a 2d viscous bi-layer shallow water model". *Nonlinear Analysis: Real World Applications*(10), pp. 2971–2984.

[8] Munoz-Ruiz, M. L., Chatelon, F. J., and Orenga, P., 2003. "On a bi-layer shallow-water problem". *Nonlinear Analysis: Real World Applications,* ***4***(1), pp. 139–171.

[9] Nouh, I., Mohammed, S., Imad, E., and Mohamed, W., 2015. "Discontinuous galerkin method for two-dimensional bilayer shallow water equations". *Journal of Engineering Mathematics*, pp. 1–21.

[10] Castro, M. J., Garcia-Rodriguez, J. A., González-Vida, J. M., Macias, J., and Parés, C., 2007. "Improved fvm for two-layer shallow-water models: Application to the strait of gibraltar". *Advances in Engineering Software,* ***38***(6), pp. 386 – 398. Advances in Numerical Methods for Environmental Engineering.

[11] Di Meglio, F., Vazquez, R., and Krstic, M., 2013. "Stabilization of a system of coupled first-order hyperbolic linear PDEs with a single boundary input". *IEEE Transactions on Automatic Control,* ***58***(12), pp. 3097–3111.

[12] Krstic, M., and Smyshlyaev, A., 2008. *Boundary control of PDEs: A course on backstepping designs*, Vol. 16. Siam.

[13] Nieto, E. F., Castro-Diaz, M. J., and Parés, C., July 2011. "On an intermediate field capturing riemann solver based on a parabolic viscosity matrix for the two-layer shallow water system". *Journal of Scientific Computing,* ***Volume 48, Issue 1-3***, pp. 117–140.

[14] Abgrall, R., and Karni, S., 2009. "Two-layer shallow water system: a relaxation approach". *SIAM J. Sci. Comput.,* ***31, No 3***, pp. 1603–1627.

[15] Schijf, J., and Schonfeld, J., Sept. (1953). "Theoretical considerations on the motion of salt and fresh water". *Proc. of the Minn. Int. Hydraulics Conv. Joint meeting IAHR and Hyd. Div. ASCE.*, pp. 321–333.

[16] LeVeque, R. J., 2002. *Finite volume methods for hyperbolic problems*. Cambridge texts in applied mathematics. Cambridge University Press, Cambridge, New York. Autres tirages : 2003, 2005, 2006.

[17] Tang, S., and Krstic, M., 2014. "Sliding mode control to the stabilization of a linear $2\times$ 2 hyperbolic system with boundary input disturbance". In American Control Conference (ACC), IEEE, pp. 1027–1032.

[18] Marx, S., Tang, S., and Krstic, M., 2016. "Stabilizing a linear KdV equation with boundary input disturbance by sliding mode control". *Submitted to the IEEE Conference on Decision and Control, under review*.

[19] Tang, S., Guo, B.-Z., and Krstic, M., 2014. "Active disturbance rejection control for 2×2 hyperbolic systems with input disturbance". In IFAC World Congress, pp. 1027–1032.